Chapter 3
Advances in Plasmonic Substrate-Coupled Fluorescence

Sharmistha Dutta Choudhury (ORCID)

3.1 Introduction

Plasmonics is a burgeoning field of nanoscience that deals with localization and guiding of light by interaction with metallic nanostructures (Schuller et al. 2010; Atwater 2007). The optical response of plasmonic materials depends on their frequency dependent dielectric function, ($\varepsilon(\omega) = \varepsilon'(\omega) + i\varepsilon''(\omega)$), that is commonly characterized by the Drude model (Maier 2007) as,

$$\varepsilon(\omega) = \left(1 - \frac{\omega_p^2}{\omega^2 + \gamma^2}\right) + i\left(\frac{\omega_p^2 \gamma}{\omega^3 + \omega\gamma^2}\right) \qquad (3.1)$$

Here ω is the angular frequency of light, γ is electron collision frequency and ω_p, is the bulk plasma frequency of the metal ($\omega_p = \sqrt{\frac{Ne^2}{m_{eff}\varepsilon_0}}$, where ε_0 is the permittivity of free space, N is the electron density, m_{eff} is the effective mass of an electron and e is the electron charge). When the frequency of incident light is above ω_p, the electrons are unable to oscillate in response to the incident field. In this condition, the real part of the dielectric constant of the metal ($\varepsilon'(\omega)$) is positive, and light is either transmitted or absorbed due to interband transitions. When the frequency of light is below ω_p, the free conduction electrons oscillate in a phase opposite to that of the incident electromagnetic field. In this case, $\varepsilon'(\omega)$ is negative and light is reflected by the metal (Figs. 3.1a and b) (Maier 2007; Li et al. 2015).

If the metal dimensions are brought down to the nano regime, two types of plasmonic modes can be generated upon interaction with light, depending on the shape

S. Dutta Choudhury (✉)
Radiation & Photochemistry Division, Bhabha Atomic Research Centre, Mumbai 400085, India
e-mail: sharmidc@barc.gov.in

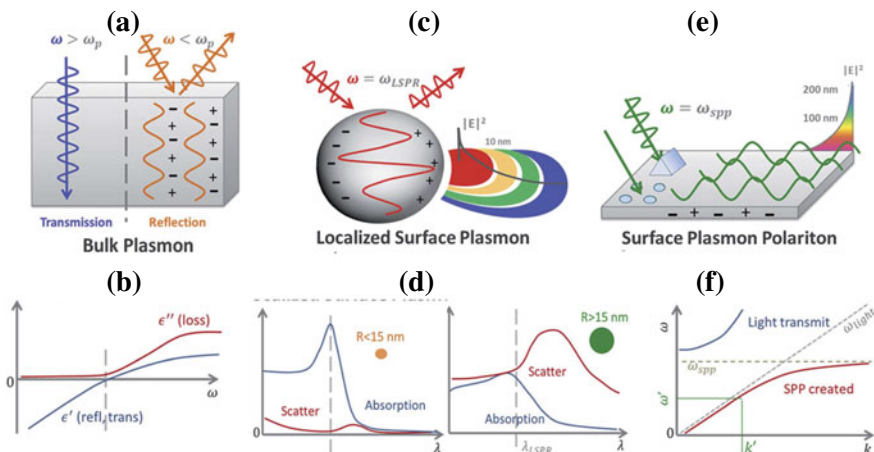Homi Bhabha National Institute, Anushaktinagar, Mumbai 400094, India

Fig. 3.1 a Interaction of light with bulk metal at frequencies below and above its plasma frequency, ω_p, and **b** complex dielectric of the metal. **c** Localised surface plasmons (LSPs) in metal nanoparticle and **d** LSP resonances due to absorption and scattering in particles of different sizes. **e** Propagating surface plasmon polaritons (SPPs) on a thin metal film and **f** the dispersion curve for SPPs. Adapted with permission from Li et al. (2015). Copyright 2015 The Royal Society of Chemistry

and size of the particles. These are: Localized Surface Plasmons (LSPs) and Surface Plasmon Polariton (SPPs).

The LSPs are collective oscillations of surface electrons that arise when the dimensions of metal nanostructures are smaller than the wavelength of light (Fig. 3.1c). LSPs can be directly excited by the incident light. From Mie theory, the extinction coefficient (σ_{ext}) of a metal nanosphere, of volume V in a medium of dielectric constant, $\varepsilon(\omega)_{diel}$, is (Link and El-Sayed 2003):

$$\sigma_{ext} = 9\frac{\omega}{c}(\varepsilon(\omega)_{diel})^{3/2}V\frac{\varepsilon(\omega)''_{metal}}{\left(\varepsilon(\omega)'_{metal} + 2\varepsilon(\omega)_{diel}\right)^2 + \left(\varepsilon(\omega)''_{metal}\right)^2} \quad (3.2)$$

When the real part of the dielectric constant, $\varepsilon(\omega)'_{metal}$, is negative and satisfies the condition, $\varepsilon(\omega)'_{metal} = -2\varepsilon(\omega)_{diel}$, and the imaginary part is small ($\varepsilon(\omega)''_{metal} \approx 0$), the denominator in Eq. 3.2 vanishes, leading to strong plasmon resonance at $\omega_{LSP} = \frac{\omega_p}{\sqrt{1+2\varepsilon(\omega)_{diel}}}$. The extinction coefficient (σ_{ext}) in Eq. 3.2 arises due to both scattering and absorption of light. With increase in size of the nanoparticle, the contribution of the scattering component in σ_{ext} gradually increases (Fig. 3.1d). An important outcome of the confined LSP oscillations is that it leads to intense local electromagnetic fields in the vicinity of the nanoparticle.

Unlike LSPs, the SPPs are propagating charge oscillations on the surface of metallic nanostructures like thin continuous metal films, whose dimensions are greater than the wavelength of light (Fig. 3.1e). The wave vector or momentum of propagating SPPs is expressed as:

$$k_{SPP} = \frac{\omega}{c} \sqrt{\frac{\varepsilon(\omega)_{metal} + \varepsilon(\omega)_{diel}}{\varepsilon(\omega)_{metal}\varepsilon(\omega)_{diel}}} \tag{3.3}$$

The resonance condition for SPPs is, $\omega_{SPP} = \frac{\omega_p}{\sqrt{1+\varepsilon(\omega)_{diel}}}$ Maier 2007; Lakowicz 2006a). Evidently, k_{SPP} is greater than the wavevector of the photon in free space ($k_0 = \frac{\omega}{c}$). So the light line lies above the dispersion curve for SPPs (Fig. 3.1f). This means that SPPs cannot be excited directly by incident light. Special conditions requiring gratings, surface corrugations, or prisms are used to excite SPPs by increasing the momentum of the incident light to match with the SPP. The wavevector matching conditions between light and SPPs implies that SPPs at the the metal–dielectric interface can exist only for TM (transverse magnetic; electric field parallel to plane of incidence) or P-polarization of light. The evanescent field of SPPs extends to a distance of about 100–200 nm from the metal film surface.

The unique features of surface plasmon resonances (LSPs and SPPs), specifically, their sensitivity to the surrounding dielectric medium, local field enhancement and creation of evanescent wave on the surface of metal nanostructures, have opened the doors for numerous applications of plasmonics. Surface enhanced Raman spectroscopy, optical sensing, photovoltaics, lasers, quantum computing, are some of the notable areas that have hugely benefitted by contribution from plasmonics (Schuller et al. 2010; Atwater 2007; Li et al. 2015; Yu et al. 2019). The entry of plasmonics in fluorescence spectroscopy is another important development that has seen remarkable progress in recent years.

Fluorescence is the emission of light by radiative relaxation of electronically excited species from their first singlet state to the ground state (Fig. 3.2) (Lakowicz 2006b). It is an indispensable tool in bioanalysis, microscopy, diagnosis and sensing, due to its great versatility, sensitivity, simplicity, and rapid noninvasive measurement technique. The extremely high sensitivity of fluorescence has permitted extraordinary developments in single molecule detection and super-resolution microscopy making it valuable for understanding complex phenomena in great detail.

Fig. 3.2 Simplified Jablonski diagram showing the first excited singlet and triplet states and the major photophysical processes in a fluorescent molecule
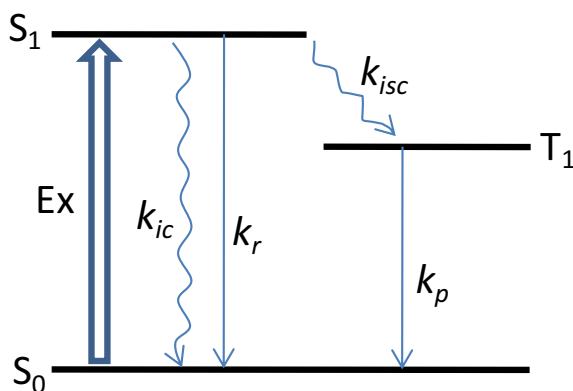
Fluorescence is characterized by two important parameters; the fluorescence quantum yield (Φ) and the fluorescence lifetime (τ), which are expressed in terms of the radiative decay rate (k_r) and nonradiative decay rate (k_{nr}) (Lakowicz 2006b).

$$\Phi = \frac{k_r}{k_r + k_{nr}} \tag{3.4}$$

$$\tau = \frac{1}{k_r + k_{nr}} \tag{3.5}$$

The nonradiative decay rate ($k_{nr} = k_{ic} + k_{isc}$) includes both intersystem crossing (*isc*) and internal conversion (*ic*). Most of the commonly known fluorophores have aromatic structures or conjugated carbon chains. Apart from molecular fluorophores, many other photoluminescent materials and quantum emitters like, semiconductor quantum dots, metal nanoclusters, upconverting rare-earth phosphors, carbon dots and perovskite nanocrystals have also been developed over the years to meet the growing demands and applications of fluorescence spectroscopy. Despite many developments, classical fluorescence, which relies on measuring the spontaneous emission of light in an optically transparent medium in the far field, is limited by challenges due to weak emission intensities, poor photostability and low collection efficiency.

Under steady state conditions, the emission photon count rate for a single fluorescent molecule (CR) is (Jiao et al. 2017),

$$CR = k_c \phi \frac{\sigma I_e}{1 + I_e/I_s} \tag{3.6}$$

Here, k_c is the light collection efficiency of the optical system, I_e is the excitation rate, σ is the absorption cross-section and I_s is the saturation intensity ($I_s = (k_r + k_{nr})/[\sigma(1 + k_{nr}/k_p)]$, where k_p is the radiative relaxation of the triplet state). Since classical fluorescence is isotropic in nature, less than 1% of the emitted light can be detected in a standard spectro-fluorometer setup (Lakowicz 2004). Moreover, bulky optical components are required to focus and collect the emitted light, which makes it difficult to progress toward device miniaturization, work with small sampling volumes and meet point-of-care requirements. With the integration of plasmonics in fluorescence, it has become possible to surpass many of the limitations of classical fluorescence and achieve enhanced brightness, better photostability and improved collection efficiency. Plasmonic coupling offers the opportunity to control emission at a fundamental level by modifying the radiative decay rates of fluorophores. Moreover, plasmonics enables emission to be controlled at the point of origin, without any external optics.

3.2 Mechanism and Effects of Fluorophore-Plasmon Interactions

Fluorophores interact with metal nanoparticles that support LSPs and metal nano films that support SPPs, leading to different kinds of effects. While the interaction with LSPs is useful for fluorescence enhancement and tailoring of radiative decay rates (Lakowicz 2006a), the interaction with SPPs is useful for transforming isotropic emission into directional, polarized and wavelength-resolved emission (Lakowicz 2004). The evanescent waves of SPPs are also used to obtain increased excitation fields for improving fluorescence signal in free space (Wang et al. 2010). The different kinds of interactions and effects observed in plasmon-coupled emission are discussed below.

3.2.1 Interaction with Metal Nanoparticles

The interaction between fluorophores and metal nanoparticles can be described as a combination of several different effects: (i) local field enhancement in the vicinity of the nanoparticle and hence around the nearby fluorophores (plasmonic antenna effect), which leads to increased excitation rates for the fluorophores; (ii) enhanced coupling efficiency of fluorescence to the far field via LSP resonance, especially the scattering component in σ_{ext}; (iii) increase in radiative decay rate of fluorophores (known as radiative decay engineering, RDE); and (iv) increased nonradiative decay due to energy transfer from fluorophores to the metal surface leading to quenching of fluorescence, a phenomenon that occurs when fluorophores are adjacent to the metal surface (Lakowicz 2006a, 2005; Khatua et al. 2014). When the fluorophore position is more than 5 nm from the metal surface, which can be achieved by using suitable spacer layers, the quenching effect is suppressed, and the plasmon-coupled fluorophore or "plasmophore" radiates with an overall increase in fluorescence intensity due to the synergistic effects of (i), (ii) and (iii). This phenomenon is known as metal-enhanced fluorescence (MEF). The effective fluorescence enhancement, ξ is expressed as, $\xi \approx E_{exc} \times E_{em}$, where E_{exc} corresponds to the excitation enhancement and E_{em} is the overall emission enhancement.

The increase in radiative decay rate for a plasmon-coupled fluorophore can be understood from Fermi's Golden Rule (Eq. 3.7) that relates radiative rate of an excited molecule to the quantum mechanical transition probability, W_{ij}.

$$W_{ij} = \frac{2\pi}{\hbar} |\mu_{ij}|^2 \rho(v_{ij}) \tag{3.7}$$

Here μ_{ij} is the transition dipole moment connecting the initial (i) and final (j) states and $\rho(v_{ij})$ is the photonic mode density at the transition frequency. For fluorophores located within nanoscale distances from a plasmonic substrate, the local density of

Fig. 3.3 a Simplified
Jablonski diagram showing
the changes in excitation and
radiative rate for a
plasmon-coupled
fluorophore. **b** Schematic
representations of the
simultaneous increase in
intensity and decrease in
lifetime
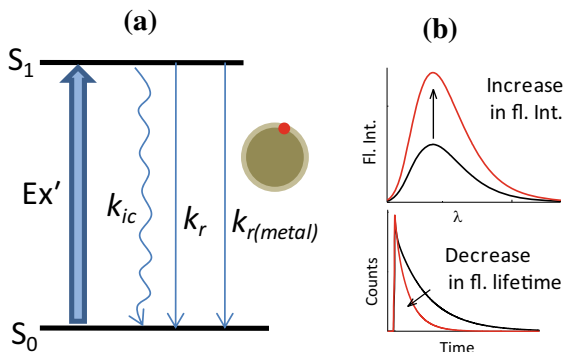
states is substantially high, which leads to increase in the radiative decay rate. An important consequence of this effect is that MEF is characterized by simultaneous increase of quantum yield (Φ_{metal}) and decrease of fluorescence lifetime (τ_{metal}) (Eqs. 3.8 and 3.9) (Lakowicz 2005; Khatua et al. 2014).

$$\Phi_{metal} = \frac{k_r + k_{r(metal)}}{k_r + k_{r(metal)} + k_{nr}} \tag{3.8}$$

$$\tau_{metal} = \frac{1}{k_r + k_{nr} + k_{r(metal)}} \tag{3.9}$$

Here $k_{r(metal)}$ is the additional increase in the radiative rate of fluorophores because of increase in the local density of states. The shortening in fluorescence lifetime is advantageous because photochemical destruction reduces for a molecule that stays for lower time in the excited state. Therefore, the enhanced fluorescence quantum yield and reduced lifetime achieved through plasmonics, greatly increases detection limit, while at the same time reducing photobleaching of fluorophores. The major photophysical changes for a plasmon-coupled fluorophore are shown in Fig. 3.3.

Observation of MEF is critically dependent on the distance between the metal nanoparticle and the fluorophores. By depositing fluorophores at different distances from metal nanostructures using Langmuir–Blodgett monolayers or polyelectrolyte layer-by-layer assembly, it has been shown that fluorescence enhancement is optimum at distances between 5 and 20 nm from the surface, where fluorophores experience enhanced excitation field intensity without being quenched by the metal (Ray et al. 2006; Akbay and Lakowicz 2012). The calculated near-field intensity map and overall fluorescence enhancement, ξ, for a fluorophore at different distances from an Au nanorod are depicted in Figs. 3.4a and 4b, respectively (Khatua et al. 2014).

MEF also depends on the shape and size of metal nanoparticles and the extent of spectral overlap between fluorescence and the LSP resonance. On comparing the fluorescence enhancement by two different Au nanostructures, viz. nanorods and nanoshells, Halas and co-workers found that the quantum yield of IR800 dye (~7%) is increased to ~86% on coupling with nanoshells whereas it increases to ~74% when
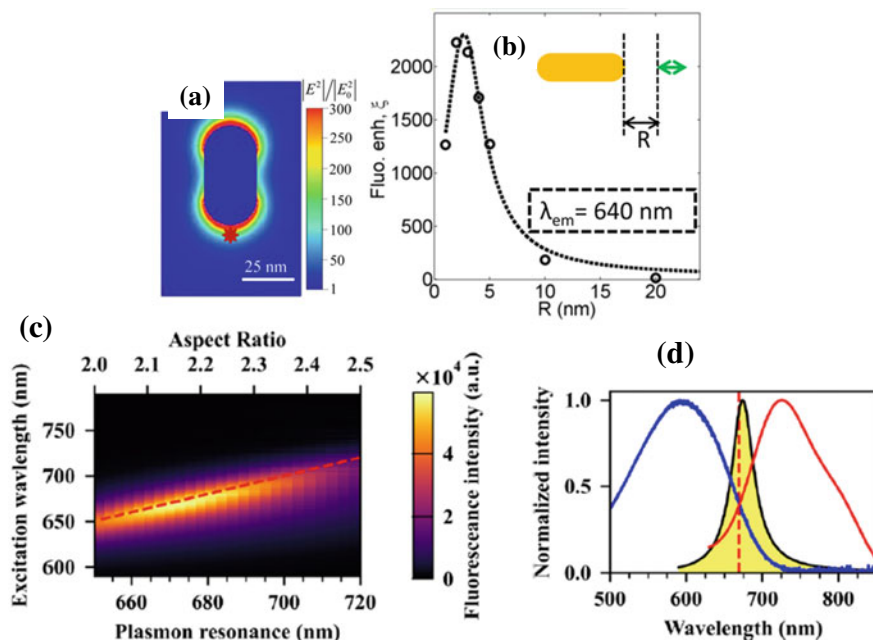
Fig. 3.4 **a** Calculated near-field intensity of an Au nanorod (47 nm long and 25 nm wide, having LSP resonance at 629 nm), and **b** calculated fluorescence enhancement, ξ, as a function of distance between the fluorophore and nanorod. Adapted with permission from Khatua et al. (2014). Lu et al. (2020) Copyright 2014 American Chemical Society. **c** Calculated enhanced emission intensity as a function of excitation wavelength and LSP resonance wavelength of Au nanorods having different aspect ratios and **d** overlap of the scattering spectra of the fabricated optimum sized Au nanorod with the absorption/emission spectra of the coupled naphthalenediimide-based NIR dye. Adapted from. Copyright 2020 American Chemical Society under Creative Commons License CC-BY-NC-ND

coupled with nanorods (Bardhan et al. 2009). This difference is ascribed to greater scattering cross-section of the LSP resonance in nanoshells compared to nanorods, at the emission wavelength of the dye. Thus, a high cross-section for scattering at the emission wavelength is favourable for efficient fluorescent enhancement. Very recently, Lu et. al. have shown that detection of single molecule fluorescence from NIR emissive dyes having quantum yield as low as 10^{-4}, is possible by coupling with Au nanorods, provided their LSP resonance is optimized with the excitation and emission wavelengths of the dye (Lu et al. 2020). Figure 3.4c shows a map of the calculated fluorescence intensity enhancement as a function of the excitation wavelength and LSP resonance for Au nanorods having different aspect ratios (length/ width of nanorod). Based on these calculations, Au nanorods of suitable geometry were fabricated so as to have maximal overlap of the plasmon resonance with the absorption/ emission spectra of the NIR dye (Fig. 3.4d), for obtaining the largest possible enhancement factor.
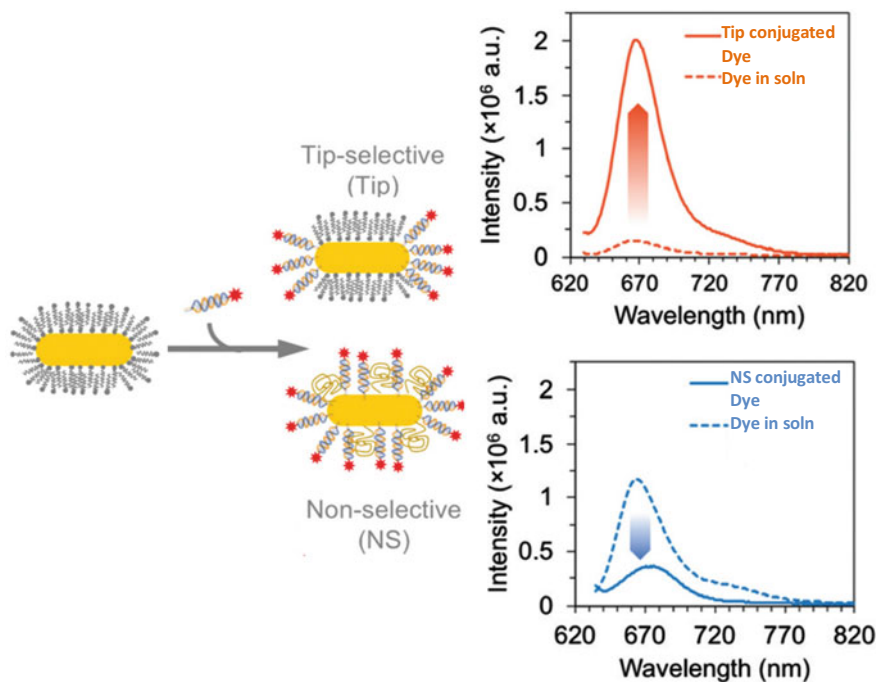
Fig. 3.5 Schematics for fluorophore conjugation specifically at the tip or non-specifically throughout the surface of Au nanorods, along with the emission spectra of the coupled fluorophore, showing enhancement and quenching effects, respectively, in the two cases. Adapted with permission from Botequim et al. (2020). Copyright 2020 The Royal society of Chemistry

The position and orientation of fluorophores on the nanoparticle is another important parameter for MEF, since the local electromagnetic field enhancement is not uniform around the nanoparticle. Higher field enhancements are observed at the tips and sharp edges around nanoparticles (cf. Fig. 3.4a). Recently, Pedro et. al. have used DNA-directed assembly to precisely position fluorescent dyes on the Au nanorod surface (Botequim et al. 2020). Their work revealed that dyes placed on the tips of the nanorods show significantly enhanced emission compared to free dyes in solution, while dyes placed in a nonspecific manner throughout the nanorod surface actually show reduced fluorescence intensity compared to that in solution (Fig. 3.5).

3.2.2 Interaction with Planar Metal Nanofilms

Although light incident directly from the far field on a thin metal film is incapable of creating SPPs on the metal–dielectric interface due to wavevector mismatch between photons and SPPs, interestingly, the emission dipoles of excited fluorophores placed

on a metal film are able to create and couple with surface plasmons in the near-field. The coupled emission can subsequently be extracted into free space by wavevector matching, using a medium with high refractive index (glass prism) (Lakowicz 2004; Gryczynski et al. 2004; Su et al. 2021).

In a medium of refractive index, n_p, the wavevector of light increases to $k = k_0 n_p$ (where $k_0 = \omega/c$ is the wavevector in air). The component along the metal surface is given as $k_x = k_0 n_p sin\theta$, where θ is the angle from the surface normal. At a certain angle θ_{sp}, the value of $k_0 n_p sin\theta$ becomes equal to k_{SPP}.

$$k_0 n_p sin\theta_{sp} = k_{SPP} = \frac{\omega}{c}\sqrt{\frac{\varepsilon(\omega)_{metal} + \varepsilon(\omega)_{diel}}{\varepsilon(\omega)_{metal}\varepsilon(\omega)_{diel}}} \qquad (3.10)$$

In this situation, the surface plasmon-coupled fluorescence can radiate through the prism as a cone of emission (in Figs. 3.6a and b). This phenomenon is known as surface plasmon-coupled emission (SPCE). Since the optical properties of the metal are frequency dependent, the emission angle θ_{sp} is also sensitive to emission wavelength. The emission at longer wavelength appears at smaller angles than that at shorter wavelength. Furthermore, since SPP can couple only with P-polarized light, the fluorescence emission is also P-polarized, even from randomly oriented fluorophores placed on the metal surface. Thus, SPCE transforms the usual isotropic unpolarized emission into a cone of wavelength-resolved, P-polarized emission.

The ability of SPCE to demarcate different wavelengths directly by their angular separation without using additional dispersive optics is promising for instrument miniaturization. Further, it allows multiple emissive species in a complex mixture to be easily sorted, based on the observation of their emissions at different angles. This has been demonstrated experimentally by Sathish et al. in the spectral resolution of emission from different Rhodamine6G dye aggregates (Sathish et al. 2009). Directional emission is another important advantage of SPCE, because signal collection efficiency can be substantially improved by aligning the detector in a specific direction (Dutta Choudhury et al. 2015a). Furthermore, since the evanescent SPP field extends to a distance of about 200 nm from the metal, SPCE allows signal from fluorophores located near the surface to be exclusively selected without perturbation from background fluorescence. This aspect has been utilised by Matveeva et. al. to carry out fluorescence immunoassays directly in human serum and whole blood without any significant attenuation of the fluorescence signal (Matveeva et al. 2005).

Two types of configurations are generally used in SPCE; the Kretschmann (KR) and the Reverse Kretschmann (RK) (Lakowicz 2004; Gryczynski et al. 2004; Su et al. 2021). In RK configuration, fluorophores are excited directly by incident light from free space and the coupled emission is subsequently collected using a prism, as depicted schematically in Fig. 3.6c. In the KR approach, fluorophores are excited by light incident through prism side. When light with excitation wavelength, λ_{ex} is incident at the correct angle (θ_{sp-ex}), SPPs can be created and fluorophores within the near-field can be excited by the evanescent field of SPPs. The emitted light can
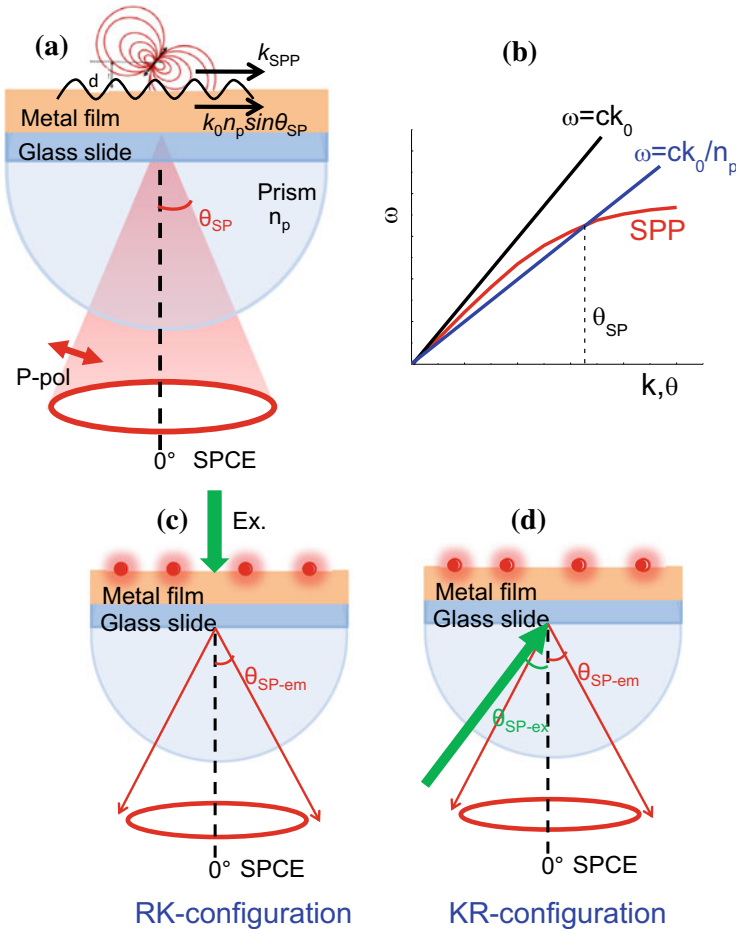
Fig. 3.6 **a** Schematic representation of SPCE, **b** the wavevector matching condition achieved by using a prism, **c** and **d** RK- and KR-configurations for SPCE

subsequently couple back with SPPs and radiate at a different angle ($\theta_{sp\text{-}em}$) corresponding to the emission wavelength, λ_{em} (Fig. 3.6d). Although the KR configuration benefits from enhanced excitation field due to creation of SPPs by the excitation light, most studies of SPCE are based on direct excitation of fluorophores in the RK configuration, because of its simplicity.

The SPCE measurements can be carried out either by angle scanning to generate angular emission patterns (Fig. 3.7a), or by leakage radiation microscopy to directly capture the image of the SPCE ring in the Fourier plane (Fig. 3.7b) (Chen et al. 2013). By changing the orientation of a polarizer placed in front of the detector, interesting variations are observed in the intensity of SPCE due to P-polarized nature of the emission.
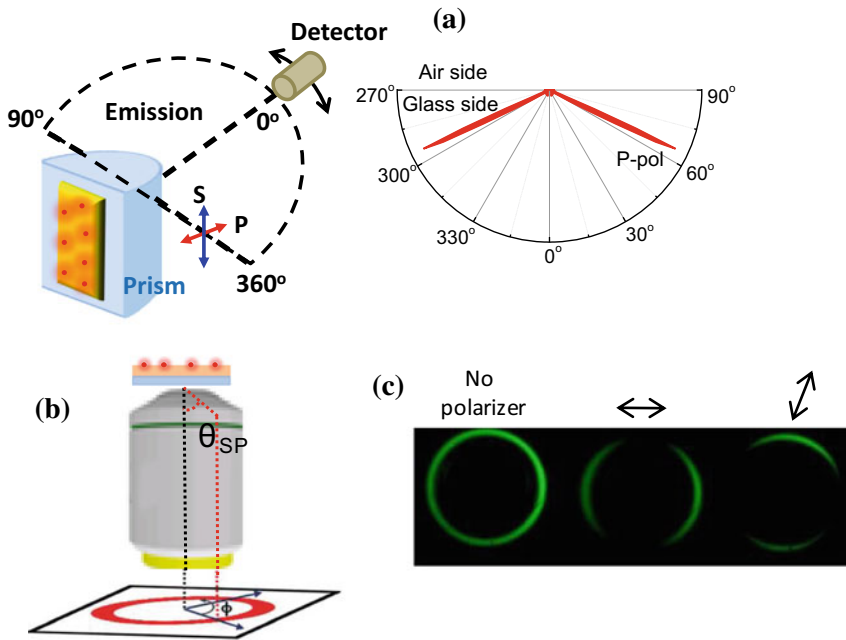
Fig. 3.7 Measurement of SPCE by **a** angle scanning to generate angular emission pattern and **b** leakage radiation microscopy to directly image the SPCE ring. **c** Images of SPCE rings with different polarizer orientations

The SPP modes in metal nanofilm substrates are often interpreted by reflectivity simulations. Light of different wavelengths is considered to be incident on the metal film at different angles through a high refractive index medium. The metal film is highly reflective at all angles above the critical angle, except for P-polarized light at $\theta_{sp\text{-}\lambda}$, when wavevector matching conditions are satisfied for creation of SPPs. Figure 3.8a depicts the calculated reflectivity dispersion map for a substrate composed of Ag film (50 nm thickness) coated with a dielectric layer (50 nm) (Dutta Choudhury et al. 2015a). The dark area is the region of decreased reflectivity due to creation of SPP. As an example, Fig. 3.8b shows that P-polarized light having wavelength of 515 nm has a dip in reflectivity at around 65°, while S-polarized light at this wavelength has a high reflectivity at all incident angles.

Interesting features appear when the dielectric layer thickness is increased in the metal-dielectric substrate, to be comparable with the wavelength of light. Now, in addition to the SPP mode, other optical modes (OMs) having both P- and S-polarizations can be sustained, with their electric fields located in different zones of the substrate (Badugu et al. 2015). The reflectivity dispersion map for such a substrate is depicted in Fig. 3.8c along with the electric field distributions corresponding to
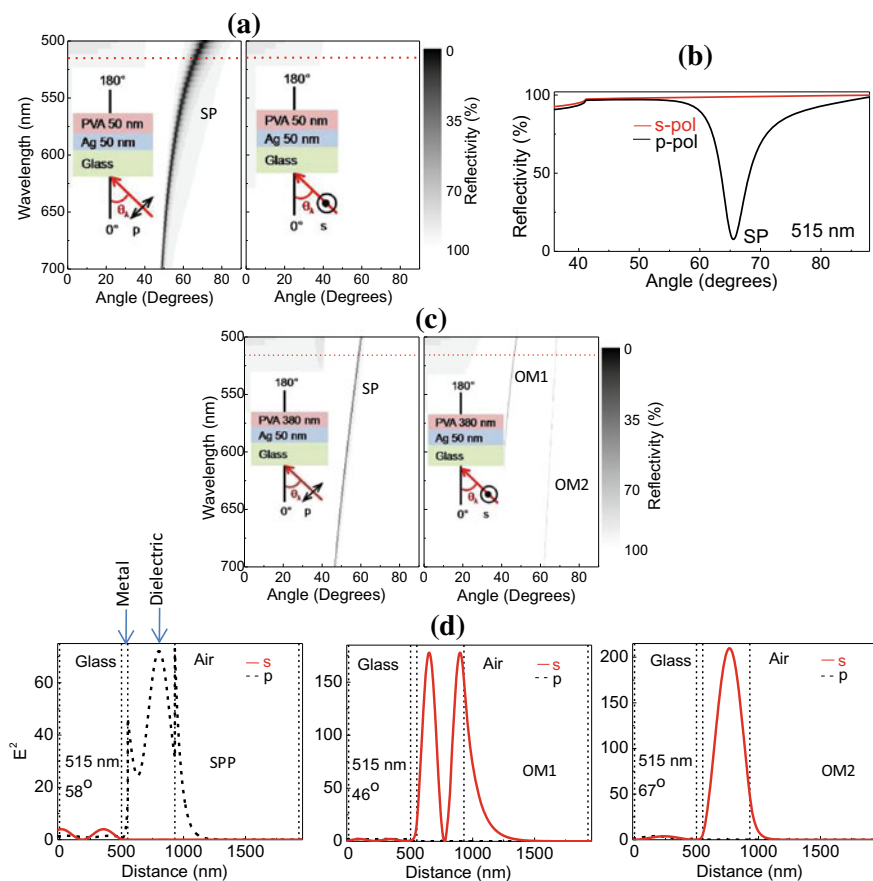
Fig. 3.8 **a** Calculated reflectivity dispersion map for a metal-dielectric substrate with dielectric thickness of 50 nm and **b** reflectivity variation with the incident angle for light having wavelength of 515 nm (corresponding to red dotted line in **a**. **c** Reflectivity dispersion map calculated for substrate with dielectric thickness of 380 nm and showing surface plasmon and OM modes. **d** The electric field intensity distributions of the optical modes in **c**. Adapted with permission from Dutta Choudhury et al. 2015a. Copyright 2015 American Chemical Society

each OM (Fig. 3.8d) (Dutta Choudhury et al. 2015a). The emission from fluorophores placed on this type of plasmon-coupled waveguide structures can interact with each of the OMs in a wavelength-dependent manner, to provide emissions at multiple angles with either S- or P-polarization. In an interesting study, this approach has been used to spectrally resolve and impart selective polarization to the intrinsically unpolarized multiple emission lines of Eu(III) ions (Dutta Choudhury et al. 2014). In another study, Lakowicz and co-workers have shown that the multiple OMs in these substrates can be exploited to selectively image emission from either the surface or the bulk, due to different polarizations and penetration depths of the OMs into the

sample space (Wang et al. 2015). This is of immense significance for monitoring weak binding events in surface-based fluorescence assays.

Another approach that combines the well established procedures of fluorescence spectroscopy with SPPs as an enhanced interfacial light source is the surface plasmon field-enhanced fluorescence (SPEF). In this case, the evanescent field of the SPPs are used for excitation of surface bound fluorophores in the KR configuration. However, unlike SPCE, instead of detecting the coupled emission, the free space emission is detected above the metal surface (Fig. 3.9a) (Neumann et al. 2002; Hageneder et al. 2021).

In the SPEF approach, plasmonic chips have been created by using different kinds of spacer molecules, so that fluorophores are placed at appropriate distances from
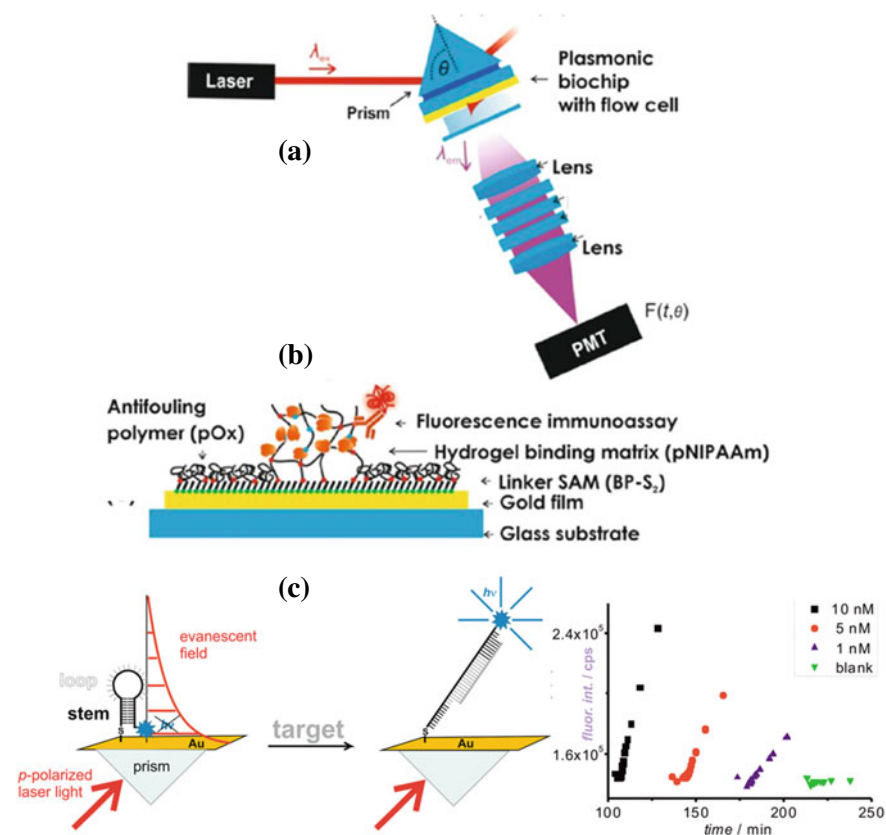

Fig. 3.9 Schematic of the optical setup for SPEF **a** and the plasmonic substrate for fluorescence immunoassay using a hydrogel binding matrix **b**. Adapted from Hageneder et al. (2021). Su et al. (2014) Copyright 2021 under Creative Commons License, published by American Chemical Society. **c** Detection and kinetic quantification of DNA target by SPEF, employing molecular beacon as a self-spacing switchable structure. Adapted with permission from. Copyright 2014 American Chemical Society

the metallic surface to avoid the quenching zone and benefit from excitation field enhancement. In this manner superior fluorescence performance and lower detection limits have been achieved in surface bound assays. Figure 3.9b shows schematics for a plasmonic biochip used for enhanced fluorescence immunoassay of human IgG antibodies for Epstein − Barr virus (EBV) (Hageneder et al. 2021). Here, the poly(N-isopropylacrylamide) (pNIPAAm)-based hydrogel serves as a binding matrix for hosting large amounts of the biomolecule. Figure 3.9c shows another example where SPEF has been used for sensitive detection and kinetic quantification of a DNA target, employing the molecular beacon as a self-spacing switchable structure (Su et al. 2014). Without DNA, the molecular beacon is in closed state, placing the fluorophores in the quenching zone of the plasmonic substrate. On binding to DNA, the molecular beacon attains an elongated double-helix structure, placing fluorophores in the plasmonically enhanced fluorescence zone, thus improving detection of the analyte. The change in fluorescence intensity was followed in real time to monitor the kinetics of binding.

3.3   Plasmonic Materials for Fluorescence Coupling

Generally, plasmonic materials are selected based on their ability to support high quality SPPs or LSP resonances, which is directly governed by the dielectric properties of the material. To quantify plasmonic performances of materials, several metrics have been defined such as the quality factor ($Q = \frac{\omega(d\varepsilon(\omega)'/d\omega)}{2\varepsilon(\omega)''}$) or the figure-of-merit ($FOM = \frac{-\varepsilon(\omega)'}{\varepsilon(\omega)''}$) (Gutiérrez et al. 2020). Important parameters that are considered in choosing the optimum plasmonic material are the plasmon resonance range, the tunability of optical properties and the losses. In metals, two types of losses are operative: the optical loss and the ohmic loss. The optical loss arises due to inter- and intra-band transitions in the metals. The ohmic loss arises due to the resistance experienced by free electrons, which is determined by the carrier concentration. A high carrier concentration implies lower losses. The plasmon resonance range is the spectral region where plasmons are resonant with incident light. This is again determined by the carrier concentration of the material. However, it can be tuned to a certain extent by controlling size, shape and assembly of the nanostructures. It may be mentioned that the plasmonic properties can also be affected by surface defects and grain boundaries. The presence of grain boundaries can impact the quality factor of the surface plasmon in thin film substrates leading to losses that are greater than theoretically calculated values. This results in reduced coupling or damping of the plasmophore emission. Figure 3.10a shows the typical plasmon spectral range of some common metals according to the shapes of their nanoparticles (Fontaine et al. 2020). Apart from plasmonic properties, other practical considerations such as stability and chemical reactivity of the material, ease of fabrication of their nanostructures and cost effectiveness are also important aspects in deciding the usefulness of a plasmonic material.
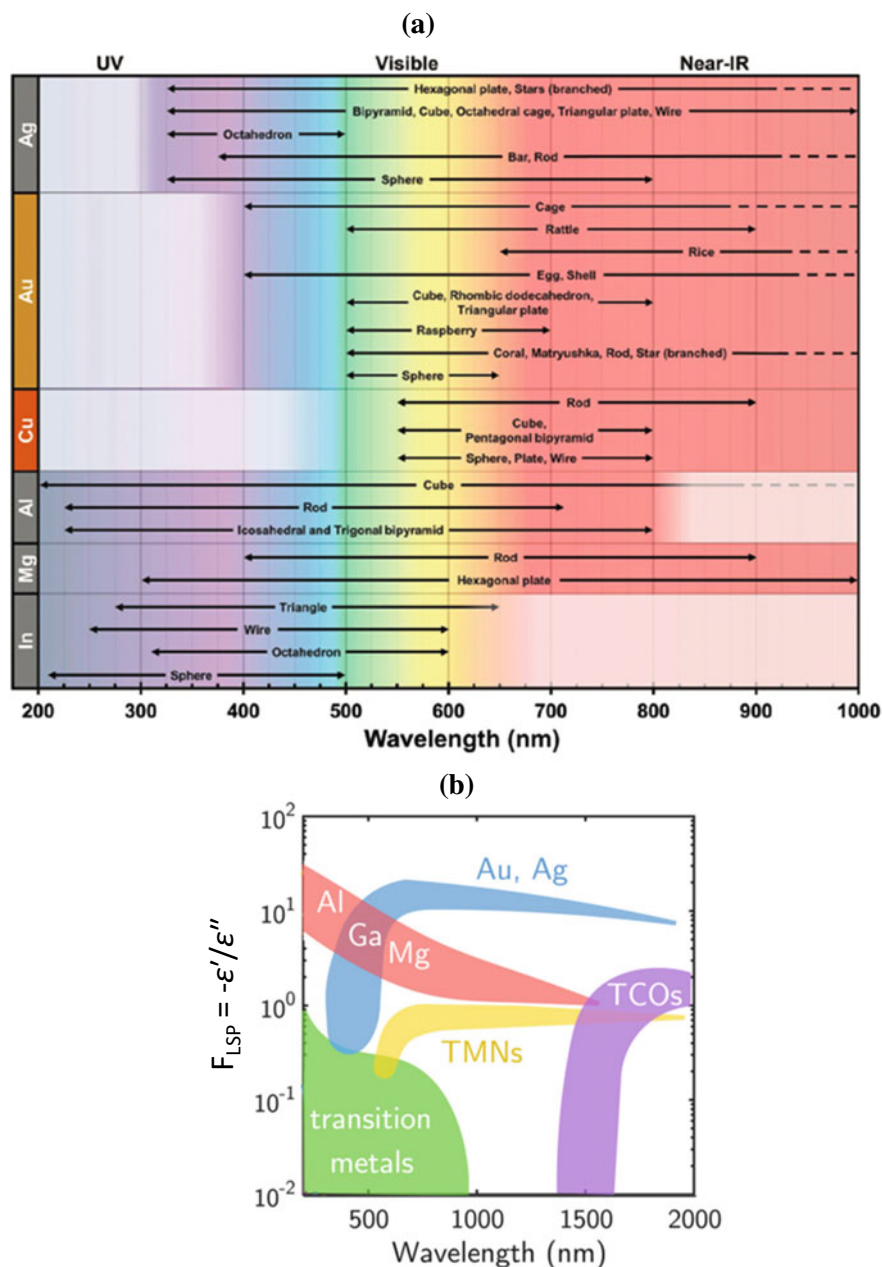
Fig. 3.10 a The plasmonic spectral range of some common metals based on the shapes of their nanostructures. Reprinted with permission from Fontaine et al. (2020). Gutiérrez et al. (2020) Copyright 2020 The Royal Society of Chemistry. **b** The plasmonic figure-of-merits for different families of materials, including noble metals, transition metals, transparent conducting oxides (TCOs) and transition metal nitrides (TMNs). Reprinted with permission from. Copyright 2020 AIP Publishing

Au and Ag are the most extensively employed noble metals for fluorescence coupling in the visible range. The quality factor of Ag is better than Au. However, Ag tarnishes easily while Au is more stable and biocompatible, though it is more expensive. Al has reasonably good plasmonic performance in the UV region. Akbay and co-workers have shown that Al and Pt nanostructures can serve as plasmonic substrates for MEF and are promising candidates for label-free detection of proteins and DNA bases that have intrinsically weak fluorescence (Akbay and Lakowicz 2012).

Despite the dominance of metals as plasmonic materials, their high optical and ohmic losses pose challenges for many plasmonic applications. Therefore, intense research is being dedicated to identify alternate plasmonic materials, having good tunability of optical properties. Graphene is a widely investigated material in this regard. However, its plasmon resonance occurs in the THz spectral range, which makes it unsuitable for fluorescence coupling (García de Abajo 2014). Doped semiconductors and transparent conducting oxides (TCOs) like, In-doped tin oxide (ITO), Al-doped ZnO (AZO), or Ga-doped ZnO (GZO) also have their plasmon resonances in the IR region (Fig. 3.10b) (Gutiérrez et al. 2020). Recently, studies have emerged that poorly plasmonic transition metals can be imparted good plasmonic properties by converting them to their nitrides and carbides. Particularly, the transition metal nitrides (TMNs), TiN, ZrN and HfN, are reported to have plasmonic resonances in the visible to NIR region (Naik et al. 2013). Interestingly, the optical response of these materials can be tuned by changing the stoichiometry of the compounds. Based on these reports, TiN substrates have been explored for SPCE and were found to be comparable to conventional Au substrate (Mishra et al. 2022). Further, the TiN substrate has the added advantage of being highly stable, and is thus suitable for reuse.

3.3.1 Fabrication of Plasmonic Substrates

While new materials continue to be investigated, Ag and Au are the most widely established metals for fabrication of plasmonic substrates for fluorescence coupling. The feasibility of making nanostructures with well-controlled morphologies has spurred the use of Ag and Au for MEF in a variety of forms, including colloidal nanoparticles in solution, films deposited on glass/quartz slides, or more complex architectures like nano arrays, plasmonic gratings and bow tie nanoantennas (Fig. 3.11) (Semeniak et al. 2022).

Colloidal nanoparticles of different morphologies like nanospheres, nanorods, nanoshells or nanocubes have been shown to provide large enhancements in fluorescence, especially by optimizing their LSP resonances with the absorption/emission spectra of the coupled fluorophores (Khatua et al. 2014; Bardhan et al. 2009; Lu et al. 2020). Some representative nanoparticles used in fluorescence coupling are shown in Fig. 3.12. Nanorods are especially attractive for MEF as their scattering spectra can be readily controlled by varying the aspect ratios (cf. Fig. 3.4c). Different
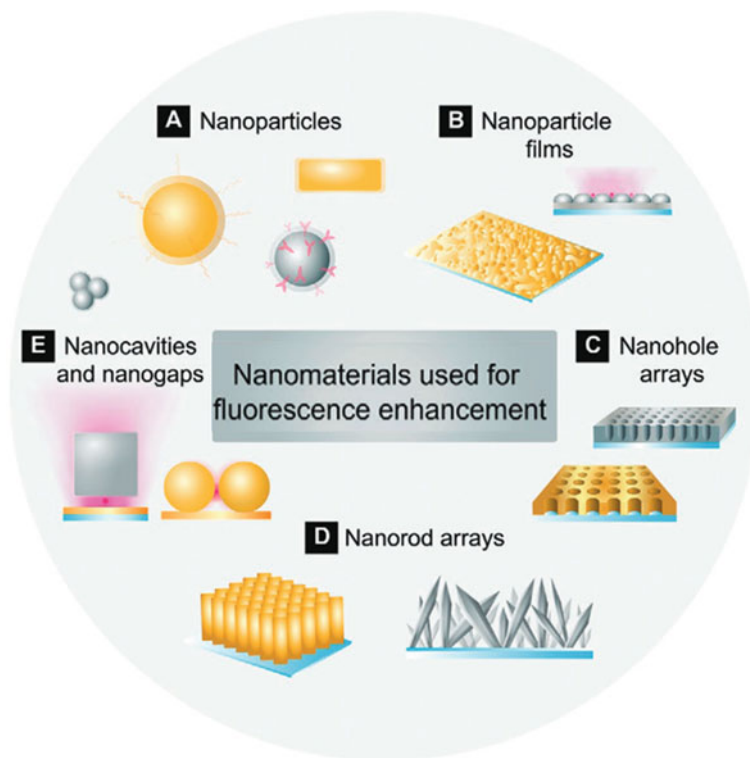
Fig. 3.11 Different kinds of plasmonic substrates used for fluorescence enhancement. Reprinted from Semeniak et al. (2022). Copyright 2022 under Creative Commons License CC BY-NC-ND 4.0, published by Wiley–VCH GmbH

wet chemical synthesis routes have been established for reproducible fabrication of nanoparticles having various shapes and sizes. Nanospheres of Ag and Au are generally obtained by the reduction of their salts ($AgNO_3$/$HAuCl_4$) with sodium citrate at controlled temperatures and reaction times, while nanorods and nanocubes are obtained by seed-mediated growth method (Rycenga et al. 2011). Metal shell-silica core nanoparticles and silica shell-metal core nanoparticles are usually prepared by the Stöber method, by using a silane agent like, 3-aminopropyltrimethoxysilane, and silicate solution or tetraethylorthosilicate as the silicon precursor (Li et al. 2017). Halas and co-workers have shown strong fluorescence enhancement in an interesting nanomatryoshka structure consisting of an Au core, an interstitial silica layer, and followed again by an Au shell layer (Orozco et al. 2014). The shell isolated nanoparticle (SHIN) is another interesting morphology for MEF, where an external silica shell is useful for controlling distance between fluorophores and nanoparticles, while at the same time allowing particle functionalization and stability. Unlike the silica shell-metal core nanoparticles prepared by Stöber method, where the silica shell is porous, the SHINs have compact and thin dielectric shells (You et al. 2020).
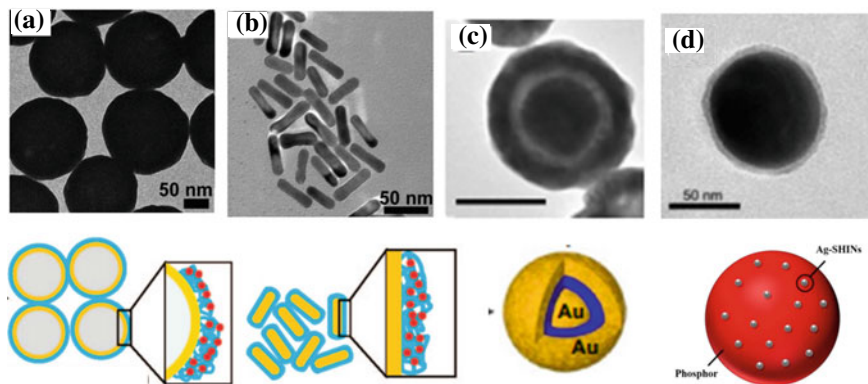
Fig. 3.12 TEM images of **a** Au nanoshells and **b** Au nanorods. Lower panel shows schematic for the conjugation of fluorescent dye on the respective nanoparticle surfaces using human serum albumin protein as spacer and linker for the dye. Reprinted with permission from Bardhan et al. (2009). Orozco et al. (2014)You et al. (2020) Copyright 2009 American Chemical Society. **c** TEM image of an Au nanomatryoshka. Lower panel shows schematic for dye doped in the interstitial SiO$_2$ layer (blue colour). Reprinted from. Copyright 2014 American Chemical Society under Creative Commons License. **d** TEM image of Ag shell isolated nanoparticle (SHIN). Lower panel shows the conjugation of Ag-SHINs with a red emissive phosphor particle through electrostatic adhesion. Reprinted with permission from. Copyright 2020 American Chemical Society

Metal nanoparticle films with rough surface morphologies can be prepared in different ways (Li et al. 2017). One approach to obtain colloid coated substrates is to first silanize a glass substrate by dipping it in 2-propanol containing (3-mercaptopropyl)trimethoxysilane, followed by immersion in an already prepared Ag or Au sol. The second approach is to deposit nanoparticles in situ by immersing the glass slides directly in the reaction mixture. Silver island films (SIFs) can be prepared in this manner by the well-known silver mirror reaction, where AgNO$_3$ is used to form Tollen's reagent, Ag(NH$_3$)$_2$OH, which is reduced subsequently to elemental Ag with glucose. The third approach is physical vapour deposition or sputtering methods to deposit a very thin discontinuous layer of Ag/Au on glass substrates. This is followed by an annealing step to generate rough surface morphologies of the metal nanoparticles on the substrates (Dutta Choudhury et al. 2012a). Figure 3.13 shows representative images of Ag nanostructures obtained by chemical reduction and thermal vapour deposition methods.

With developments in lithographic nanofabrication techniques, plasmonic substrates have progressed toward more exotic and complex architectures. A few of these structures are presented in Fig. 3.14, along with brief discussions about their effects on fluorescence.

Using electron beam lithography technique, Kinkhabwala et. al. fabricated Au bow tie nanoantenna structures (Fig. 3.14a) (Kinkhabwala et al. 2009). These nanoantennas enhanced the fluorescence intensity of NIR emissive dyes to a large extent (~1340-fold) when the dyes were optimally situated in the junction between the tips
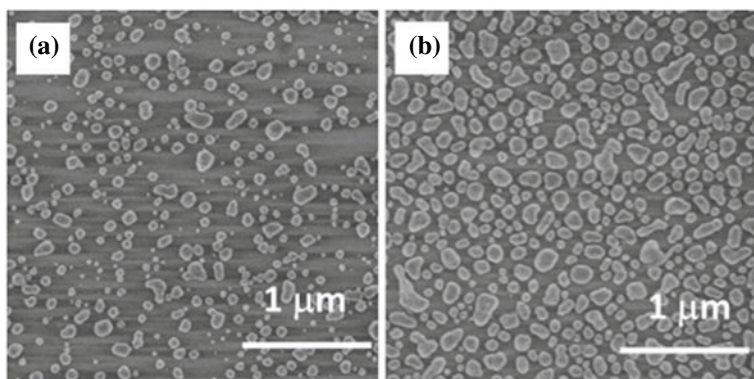
Fig. 3.13 SEM images of silver island films (SIFs) on glass slides obtained by **a** in situ silver mirror reaction and **b** thermal vapour deposition. Reprinted with permission from Dutta Choudhury et al. 2012a. Copyright 2012 American Chemical Society
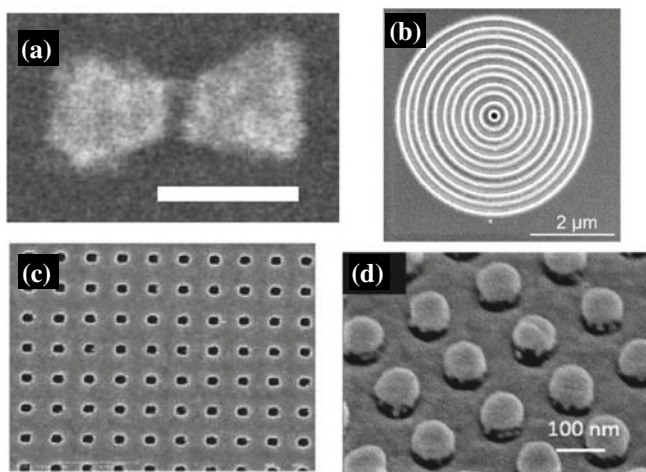

Fig. 3.14 a SEM image of Au bow tie nanoantenna fabricated by electron beam lithography. Reprinted with permission from Kinkhabwala et al. (2009). Aouani et al. (2011)Song et al. (2015)Zang et al. (2019) Copyright 2009 Nature Publishing Group. **b** SEM image of a "bulls eyes" structure fabricated by focussed ion beam milling on an Au film. Reprinted with permission from. Copyright 2011 American Chemical Society. **c** SEM image of Au nanoholes fabricated by nanoimprinting. Reprinted with permission from. Copyright 2015 Elsevier. **d** SEM image of 3D nanoantenna structure of Au nanoparticles on SiO_2 pillars fabricated by nanoimprint lithography. Reprinted with permission from. Copyright 2019 Wiley

of two triangles. These positions are the "hot spots" where enhancement of the local electric field is the highest. In another study, Aouani et. al. have used focussed ion beam milling to generate "bulls eyes" structures, which consist of nanoapertures surrounded by periodic corrugations (Fig. 3.14b) (Aouani et al. 2011). For fluorophores located near these nanoapertures, the count rate per molecule was enhanced up to 120-fold. At the same time, emission was coupled into a narrow angular cone perpendicular to the sample. Nanoimprint lithography is another technique that has been used for plasmonic substrate fabrication. Using this method, Song et. al. fabricated Au nanohole arrays (Fig. 3.14c). When applied in an aptamer-based sensor design, these nanohole arrays provided ~20 fold enhancement of quantum dot emission, which resulted in picomolar sensitivity for detection of thrombin (Song et al. 2015). More recently, Zang et al. developed a 3D nanoantenna plasmonic sensor using nanoimprint lithography, for the ultrasensitive detection of Ebola virus antigen (Zang et al. 2019). The 3D nanoantenna structure consisted of SiO_2 nanopillar array with Au nanodisks on top of each pillar, Au nanodots on the sidewalls of the pillars and an Au plane at the base (Fig. 3.14d). This plasmonic sensor platform provided a massive 240,000-fold improvement in sensitivity compared to existing methods for Ebola virus detection.

Apart from plasmonic substrates based on a single metal, bimetallic structures and metal nanocomposites have also been explored to expand the optical range of the plasmon resonance and improve the stability of the substrate. Zhang et al. prepared dielectric core-metal shell particles consisting of two concentric metallic shells, one of them Au and another Ag, by wet chemical synthesis procedures (Zhang et al. 2012). Hao et al. fabricated Al-Ag bimetallic substrates by ion implantation of Ag on an Al film. These substrates were capable of providing broadband fluorescence enhancement from UV to visible regions (Hao et al. 2014). Nanocomposite substrates of Ag and Au have also been prepared through galvanic replacement reaction by immersing a glass slide coated with Ag film into a solution of $HAuCl_4$, which led to the spontaneous replacement of Ag with Au (Fig. 3.15). This nanocomposite material provided ~50-fold enhancement for fluorophores in proximity to the hotspots in the substrate (Dutta Choudhury et al. 2012b). Single molecule fluorescence studies confirmed the increased photostability of dyes coupled to this substrate.

Unlike MEF, the substrates for SPCE are in the form of smooth continuous metal films (Fig. 3.16). In this case, large area substrate fabrication is easily achieved by sputtering or thermal vapour deposition of metallic layers (~50 nm) on glass slides, followed by deposition of a dielectric layer. The dielectric layer can be obtained by thermal vapour deposition (in the case of silica) or by spin coating (in the case of a polymer like polyvinyl alcohol, PVA) (Dutta Choudhury et al. 2015a). The thickness of the layers is controlled by controlling the deposition time, spin coating parameters and concentration of the polymer solution. Different geometries, like metal-dielectric, metal-dielectric-metal or plasmon coupled waveguide structures can be prepared to obtain SPCE or waveguide-coupled emission.
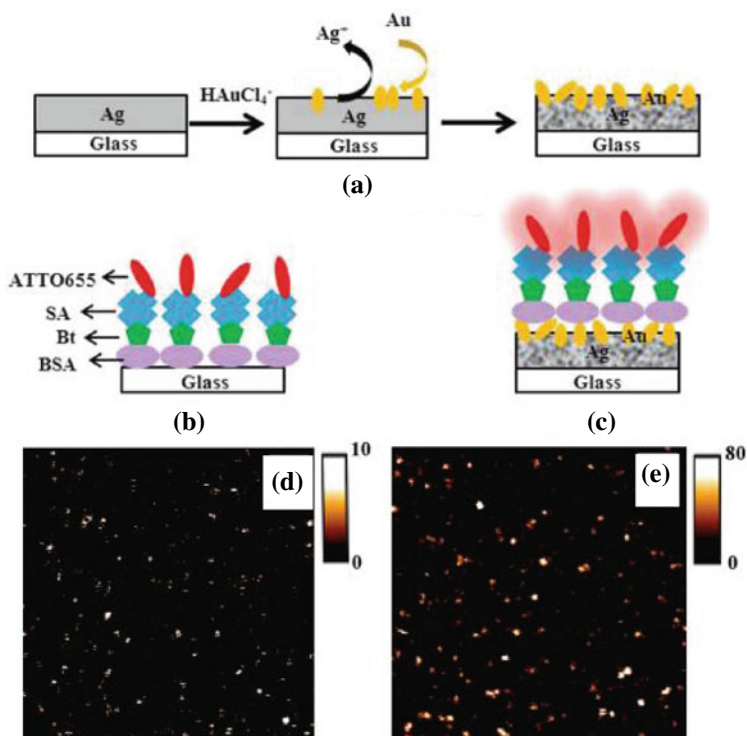
Fig. 3.15 Schematics for fabrication of Au–Ag nanocomposite substrate by galvanic replacement and conjugation of fluorophores (ATTO655) using bovine serum albumin (BSA), biotin (Bt) and streptavidin (SA) assembly **a–c**. Single molecule scanning confocal images of ATTO655 on bare glass **d** and on nanocomposite substrate **e** with respective intensity scales. Adapted with permission from Dutta Choudhury et al. 2012b. Copyright 2012 American Chemical Society

Fig. 3.16 Photographs of continuous thin layer films of **a** Au prepared by thermal vapour deposition and **b** TiN prepared by sputtering
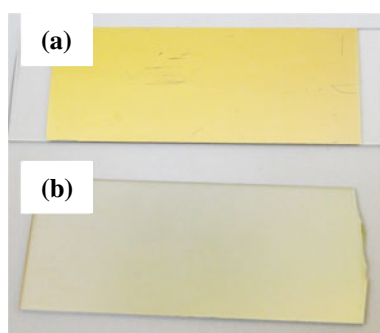
3.4 Applications of Plasmonic Substrate-Coupled Fluorescence

One of the areas where plasmon-coupled fluorescence has made a major impact is optical sensing, where it offers many-fold improvements in sensitivity over conventional fluorescence-based methods. Different kinds of analytes including toxic metals, model biomolecules (DNA, RNA, pyrophosphates, ATP etc.), various disease biomarkers and pathogens, have been detected based on the principles of plasmon-coupled fluorescence (Li et al. 2015; Hageneder et al. 2021; Su et al. 2014; Semeniak et al. 2022; Song et al. 2015; Zang et al. 2019; Wang et al. 2021; Liu et al. 2020). Importantly, plasmonic substrates can be readily incorporated into already established fluorescence technologies like, fluorescence microscopes or fluorescence plate readers to benefit from the additional enhancements provided by MEF, SPCE or SPEF.

Recently, Luan et al. have prepared a flexible nanoparticle embedded substrate that can be applied as an add-on plasmonic patch to obtain uniformly large enhancements (Luan et al. 2018). A schematic of this novel approach used for fluoro-immunoassays is shown in Fig. 3.17. The plasmonic patch was added on a standard 96-well plate with glass bottom to detect early-stage biomarkers for acute kidney injury (kidney injury molecule-1, KIM1). It was also applied in a protein microarray format to detect several protein biomarkers for kidney injury. The plasmonic patch provided more than two orders of magnitude fluorescence enhancement, ~300-fold lower limit of detection and three orders of magnitude higher dynamic range, across all assay formats.

The detection of DNA by the SPEF approach using a molecular beacon has been described earlier (cf. Fig. 3.9b) (Su et al. 2014). An alternative enhanced interfacial molecular beacon strategy for DNA/protein detection using SPCE has been demonstrated by Cao et al. In their approach, graphene oxide has been used as an additional interfacial quencher layer that works in conjunction with the plasmonic metal layer (Cao et al. 2019). In the absence of analyte, the fluorophore labelled DNA probe is in close contact with graphene oxide and the metal surface, leading to strong quenching of fluorescence. On binding to the target analyte, the conformation of the probe changes, placing the fluorophores away from the quenchers (graphene oxide and metal surface) and in the region of plasmonic enhancement (Fig. 3.18a). This results in a better contrast for the quenching-to-enhancing transition, thus improving the sensitivity of detection.

Pang et al. developed a label-free fluorescence sensor for H5N1 influenza virus, based on MEF with core–shell metal nanoparticles (Fig. 3.18b) (Pang et al. 2015). In the presence of the recombinant hemagglutinin (rHA) protein of H5N1 virus, the aptamer sensor attached to the core–shell nanoparticle acquires a G-quadruplex structure, which further binds to the dye Thiazole orange (TO) that is otherwise weekly fluorescent in the free state in solution. This sequence of events brings the dye in close proximity of the metal nanoparticle leading to a large plasmon-coupled enhancement in fluorescence signal.
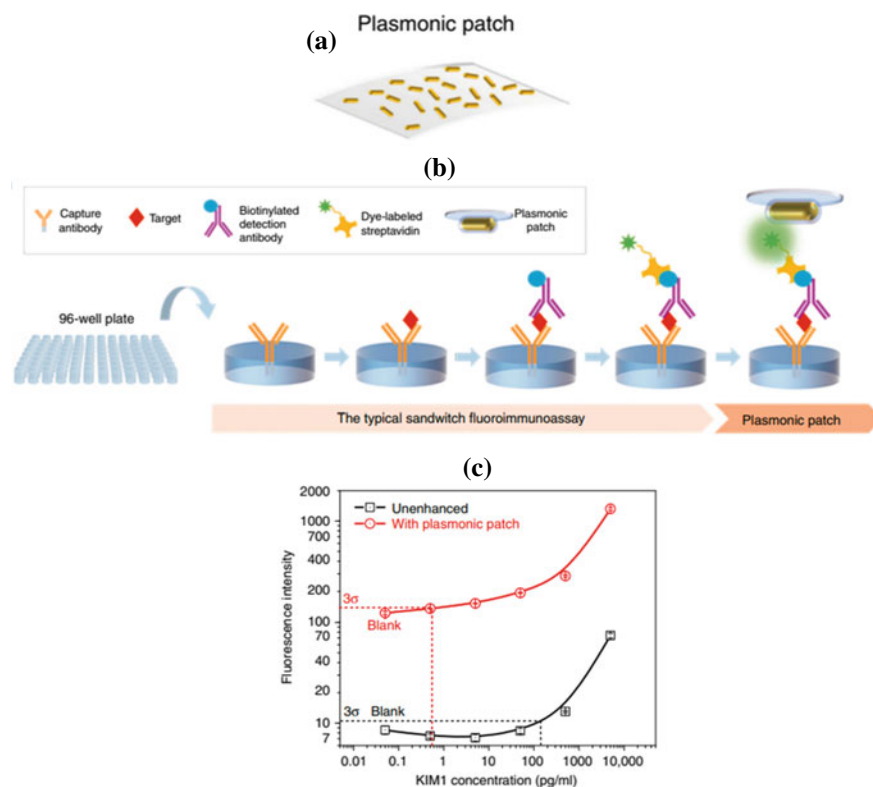
Fig. 3.17 a Representation of an add-on plasmonic patch and **b** fluoro-immunoassay using plasmonic patch. **c** Sensor response with and without the plasmonic patch. Adapted from Luan et al. (2018) under Creative Commons License, published by Springer Nature

Recently, Choi et al. have used the MEF strategy to detect cell-free DNA (cfDNA), which are important biomarkers for early stage cancer detection (Choi et al. 2020). Sensing of cfDNA is difficult because of their low abundance in blood and body fluids. Therefore, additional nucleic acid amplification steps are usually required to improve the sensitivity of detection. Choi et al. designed their sensor based on the CRISPR-Cas12a-mediated trans-cleavage reaction, where the activated CRISPR-Cas12a complex selectively degrades single-strand DNA (ssDNA) while leaving double-strand DNA (dsDNA) intact. Two Au nanoparticles (20 and 60 nm) were connected by a short ssDNA strand (2 nm) as well as a long fluorophore labelled dsDNA strand (7 nm). In this state, the fluorescence from the dye is strongly quenched due to its closeness to the 60 nm Au nanoparticle. In the presence of target cfDNA, the CRISPR-Cas12a complex is activated leading to cleavage of ssDNA and release of the fluorophore tagged 20 nm Au nanoparticle. This plasmon-coupled fluorophore is situated at an optimum distance to exhibit MEF, leading to an off-to-on transition in

Fig. 3.18 a Detection of analytes (DNA and protein) by an interfacial molecular beacon strategy using graphene oxide as a quencher, based on SPCE. Reprinted with permission from Cao et al. (2019). Copyright 2019 American Chemical Society. **b** Detection of rHA protein of H5N1 virus by aptamer sensing, based on MEF. Reprinted with permission from Pang et al. (2015). Copyright 2015 Elsevier. **c** A MEF based approach for detection of cfDNA (cancer biomarker) without involving any nucleic acid amplification step. Reprinted with permission from Choi et al. (2020). Copyright 2021 American Chemical Society
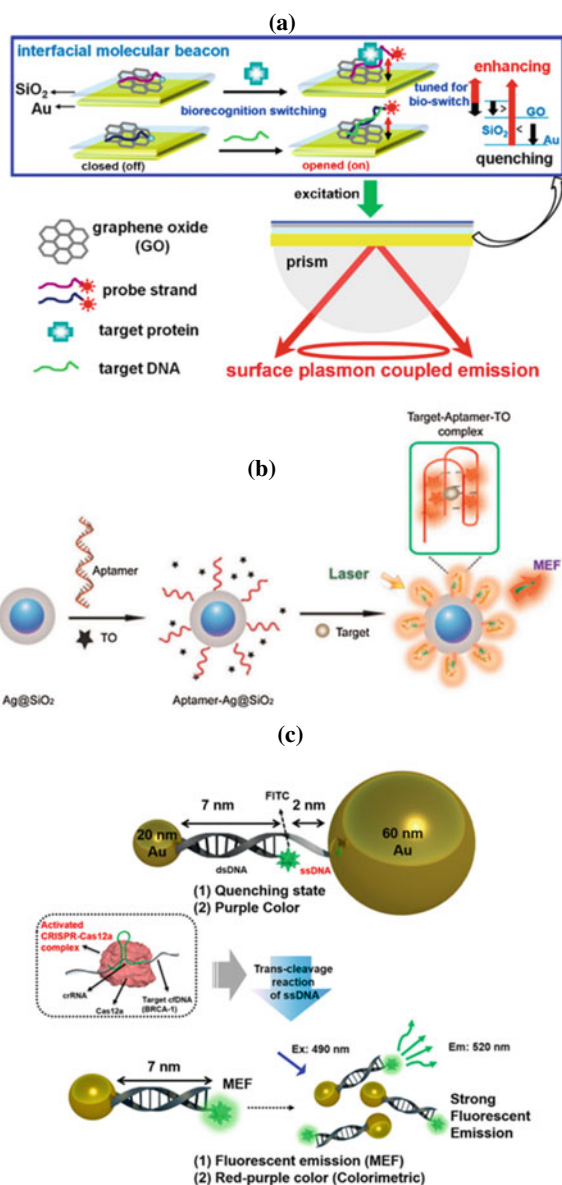
fluorescence signal. The implementation of MEF resulted in the detection of cfDNA at femtomolar concentrations without requiring any amplification steps.

In an interesting application of SPCE, Xu et al. have recently demonstrated a label-free fluorescent nanofilm sensor for in situ monitoring of the growth of metal–organic frameworks (MOF) (Xu et al. 2022). The principle behind this application is that, as the thickness of the dielectric layer above a metal nano film increases, a

plasmon-coupled waveguide structure is generated in which emission can be coupled at different angles and with both S- and P-polarizations. The study was carried out in the RK configuration. A thin layer of Rhodamine B dye was first coated on to an Au film, and a zeolite imidazolate MOF film was grown on this substrate. The thickness of the MOF film could be sensitively characterized by the unique angle distribution and polarization of the coupled emission from Rhodamine B (Fig. 3.19).

Single molecule detection is another important application of plasmonic substrate-coupled fluorescence. Several studies have been carried out to optimize the parameters of metal nanostructures (shape, assembly, position of LSP resonances) that can provide the largest enhancement factors to improve the detectability of single fluorescent molecules with low quantum yields (Bardhan et al. 2009; Lu et al. 2020; Dutta Choudhury et al. 2012a; Kinkhabwala et al. 2009). Plasmonic coupling is also useful for fluorescence correlation spectroscopy (FCS), which is an important bioanalytical technique for studying molecular interactions and dynamics based on fluorescence intensity fluctuations in a small detection volume. Plasmonic nanoapertures have been found to reduce the detection volumes so that measurements can be carried out at high concentrations that are more relevant to the realistic biological concentration range. Besides physical confinement within the nanoapertures, the volume reduction also arises because of the creation of a highly fluorescent zone in the vicinity of the nano structures due to MEF effect (Dutta Choudhury et al. 2012a; Winkler et al. 2018). This increases fluorescence count rates and improves detection of single diffusing molecules.
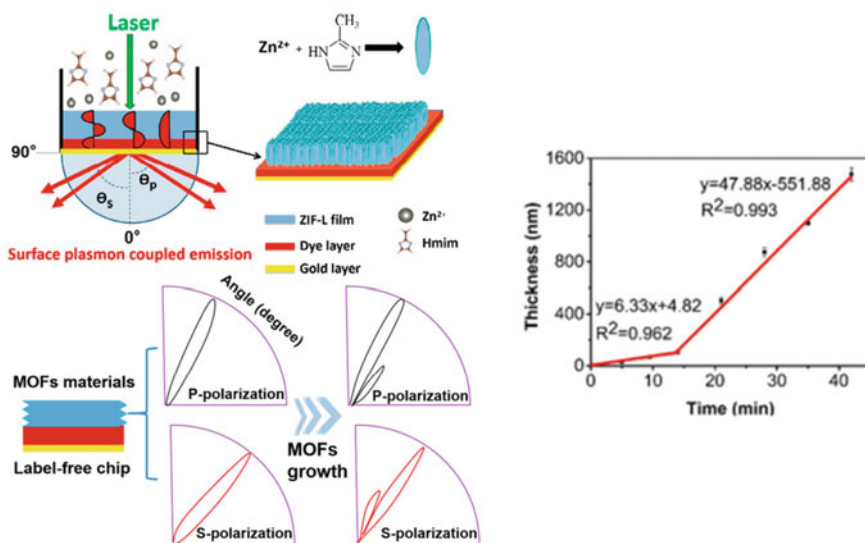

Fig. 3.19 Application of SPCE for in situ monitoring of the growth of metal–organic framework (MOF) layer. Reprinted with permission from Xu et al. (2022). Copyright 2022 American Chemical Society
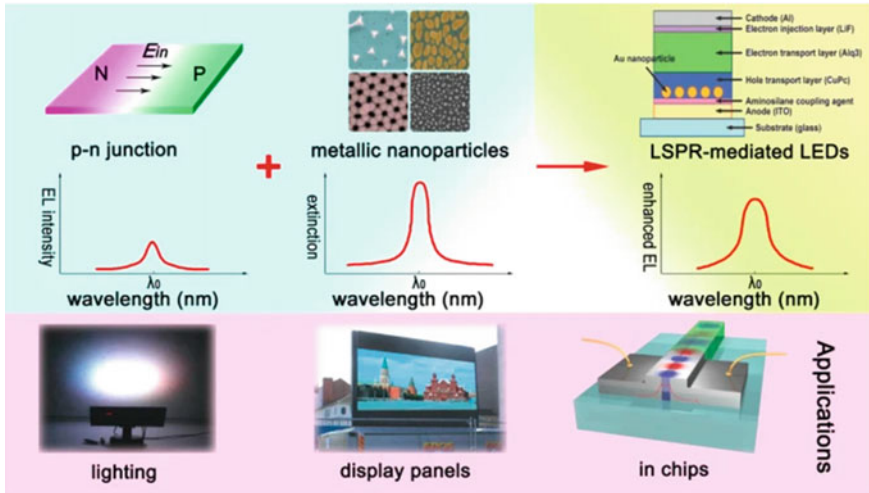
Fig. 3.20 Schematic of plasmon-coupled luminescence in LEDs and its prospective applications in display technologies. Reprinted from Gu et al. (2011). Copyright 2011 under Creative Commons License, published by Springer

Plasmon-coupled fluorescence is also being explored in the field of display technologies. The angle and thickness dependent emission in metal-dielectric-metal and plasmon-coupled waveguide structures is relevant for optical signage applications (Dutta Choudhury et al. 2015b). Plasmonic light emitting diodes (LEDs) are of immense interest for enhancing the efficiency and intensity of conventional LEDs by coupling of excitons with LSPs in metal nanoparticles (Fig. 3.20) (Gu et al. 2011; Okamoto et al. 2017). You et al. have shown that large enhancement in emission of phosphors (which are an integral component of LEDs) can be achieved by coupling with the LSP of shell isolated nanoparticles, Ag-SHINs (cf. Fig. 3.12d) (You et al. 2020). Although there are many challenges in the design and fabrication of optimum structures, plasmonic coupling has the potential to enable high efficiency, energy saving emissive devices in the future.

3.5 Conclusions and Perspectives

The coupling of fluorescence with plasmonics has allowed nanoscale imaging and detection of emission with high efficiency. The unique optical properties of plasmonic nanostructures and a fundamental understanding of metal-fluorophore interactions has generated a wealth of information for developing new generation of fluorescence probes with applications in healthcare and environmental monitoring, as well as in the design of energy saving display technologies.

Surface plasmon resonances can concentrate and magnify the incident electromagnetic field and modulate the fluorescence parameters to enable ultrasensitive detection. This overcomes limitations like, insufficient sensitivity, low specificity, and requirement of amplification steps to multiply and quantify biological species that are in low abundance. The compatibility of plasmonic sensing with portable platforms can accelerate the transformation toward wearable devices and point-of-care kits. We can also look forward to plasmophore coupled nanoscale endoscopic tools that will enable interrogation of small volumes and in vivo applications. The arrival of new plasmonic materials besides metals will facilitate adequate choice of materials and functions for application based structure design. It is anticipated that with progress in the nanofabrication methods, more complex nano architectures will be possible and advanced simulation and machine learning tools will help in assessing the efficacy of a plasmonic structure for fluorescence modulation before its fabrication. The field of plasmon-coupled fluorescence is expanding into diverse areas of material and biological sciences. As the world recovers from the devastating effects of COVID-19, it is quite clear that fast and accurate diagnostic systems are urgently needed to tackle fast-spreading infectious diseases and increase our preparedness for the future. In this regard, plasmon-enhanced fluorescence biosensors hold great promise due to their easy integration with established fluorescence spectroscopy techniques, simple instrumentation and minimal sample pre-treatment.

References

Akbay, N., Lakowicz, J.R.: Ray K (2012) Distance-dependent metal-enhanced intrinsic fluorescence of proteins using polyelectrolyte layer-by-layer assembly and aluminum nanoparticles. J. Phys. Chem. C **116**, 10766–10773 (2012)

Aouani, H., Mahboub, O., Bonod, N., Devaux, E., Popov, E., Rigneault, H., Ebbesen, T.W., Wenger, J.: Bright unidirectional fluorescence emission of molecules in a nanoaperture with plasmonic corrugations. Nano Lett. **11**, 637–644 (2011)

Atwater, H.A.: The promise of plasmonics. Sci. Am. **17**, 56–63 (2007)

Badugu, R., Szmacinski, H., Ray, K., Descrovi, E., Ricciardi, S., Zhang, D., Chen, Y., Huo, Y., Lakowicz, J.R.: Fluorescence spectroscopy with metal−dielectric waveguides. J. Phys. Chem. C **119**, 6245–16255 (2015)

Bardhan, R., Grady, N.K., Cole, J.R., Joshi, A., Halas, N.: Fluorescence enhancement by Au nanostructures: nanoshells and nanorods. ACS Nano **3**, 744–752 (2009)

Botequim, D., Silva, I.I.R., Serra, S.G., Melo, E.P., Prazeres, D.M.F., Costa, S.M.B., Paulo, P.M.R.: Fluorescent dye nano-assemblies by thiol attachment directed to the tips of gold nanorods for effective emission enhancement. Nanoscale **12**, 6334–6345 (2020)

Cao, S.H., Weng, Y.H., Xie, K.X., Wang, Z.C., Pan, X.H., Chen, M., Zhai, Y.Y., Xu, L.T., Li, Y.Q.: Surface plasmon coupled fluorescence-enhanced interfacial "molecular beacon" to probe

biorecognition switching: an efficient, versatile, and facile signaling biochip. ACS ApplBio Mater **2**, 625–629 (2019)

Chen, Y., Zhang, D., Han, L., Rui, G., Wang, X., Wang, P., Ming, H.: Surface-plasmon-coupled emission microscopy with a polarization converter. Opt. Lett. **38**, 736–738 (2013)

Choi, J.H., Lim, J., Shin, M., Paek, S.H., Choi, J.W.: CRISPR-Cas12a-based nucleic acid amplification-free DNA biosensor via Au nanoparticle-assisted metal-enhanced fluorescence and colorimetric analysis. Nano Lett. **21**, 693−699 (2020)

Dutta Choudhury, S., Ray, K., Lakowicz, J.R.: Silver nanostructures for fluorescence correlation spectroscopy: reduced volumes and increased signal intensities. J. Phys. Chem. Lett. **3**, 2915–2919 (2012a)

Dutta Choudhury, S., Badugu, R., Ray, K., Lakowicz, J.R.: Silver−gold nanocomposite substrates for metal-enhanced fluorescence: ensemble and single-molecule spectroscopic studies. J. Phys. Chem. C **116**, 5042–5048 (2012b)

Dutta Choudhury, S., Badugu, R., Lakowicz, J.R.: Surface-plasmon induced polarized emission from Eu(III)—a class of luminescent lanthanide ions. Chem. Commun. **50**, 9010–9013 (2014)

Dutta Choudhury, S., Badugu, R., Lakowicz, J.R.: Directing fluorescence with plasmonic and photonic structures. Acc. Chem. Res. **48**, 2171–2180 (2015a)

Dutta Choudhury, S., Badugu, R., Ray, K., Lakowicz, J.R.: Directional emission from metal−dielectric−metal structures: effect of mixed metal layers, dye location, and dielectric thickness. J. Phys. Chem. C **119**, 3302–3311 (2015b)

Fontaine, N., Picar-Lafond, A., Asselin, J., Boudreau, D.: Thinking outside the shell: novel sensors designed from plasmon-enhanced fluorescent concentric nanoparticles. Analyst **145**, 5965–5980 (2020)

García de Abajo 2014 García de Abajo, F.J.: Graphene plasmonics: challenges and opportunities. ACS Photon. **1**, 135–152 (2014)

Gryczynski, I., Malicka, J., Gryczynski, Z., Lakowicz, J.R.: Radiative decay engineering 4. Experimental studies of surface plasmon-coupled directional emission. Anal. Biochem. **324**, 170–182 (2004)

Gu, X., Qiu, T., Zhang, W., Chu, P.K.: Light-emitting diodes enhanced by localized surface plasmon resonance. Nanoscale Res. Lett. **6**, 199 (2011)

Gutiérrez, Y., Brown, A.S., Moreno, F., Losurdo, M.: Plasmonics beyond noble metals: exploiting phase and compositional changes for manipulating plasmonic performance. J. Appl. Phys. **128**, 080901 (2020)

Hageneder, S., Jungbluth, V., Soldo, R., Petri, C., Matthias, P., Kreivi, M., Weihaüsel, A., Jonas, U., Dostalek, J.: Responsive hydrogel binding matrix for dual signal amplification in fluorescence affinity biosensors and peptide microarrays. ACS Appl. Mater. Interfaces **13**, 27645–27655 (2021)

Hao, Q., Du, D., Wang, C., Li, W., Huang, H., Li, J., Qiu, T., Chu, P.K.: Plasmon-induced broadband fluorescence enhancement on Al-Ag bimetallic substrates. Sci. Rep. **4**, 6014 (2014)

Jiao, X., Wang, Y., Blair, S.: Plasmonic enhancement of UV fluorescence. In: Geddes, C.D., (ed.), Surface Plasmon Enhanced, Coupled and Controlled Fluorescence, Chap 18, pp. 295–308. John Wiley & Sons, Inc. USA (2017)

Khatua, S., Paulo, P.M.R., Yuan, H., Gupta, A., Zijlstra, P., Orrit, M.: Resonant plasmon enhancement of single-molecule fluorescence by individual gold nanorods. ACS Nano **8**, 4440–4449 (2014)

Kinkhabwala, A., Yu, Z., Fan, S., Avlasevich, Y., Müllen, K., Moerner, W.E.: Large single-molecule fluorescence enhancements produced by a bowtie nanoantenna. Nat. Photonics **3**, 654–657 (2009)

Lakowicz, J.R.: Radiative decay engineering 3. Surface plasmon-coupled directional emission. Anal. Biochem. **324**, 153–169 (2004)

Lakowicz, J.R.: Radiative decay engineering 5: Metal-enhanced fluorescence and plasmon emission. Anal. Biochem. **337**, 171–194 (2005)

Lakowicz, J.R.: Plasmonics in biology and plasmon-controlled fluorescence. Plasmonics **1**, 5–33 (2006a)

Lakowicz, J.R.: Principles of Fluorescence Spectroscopy, 3rd edn. Publisher, Springer, Singapore (2006b)

Li, M., Cushing, S.K., Wu, N.: Plasmon-enhanced optical sensors. Analyst **140**, 193–406 (2015)

Li, J.F., Li, C.Y., Aroca, R.F.: Plasmon-enhanced fluorescence spectroscopy. Chem. Soc. Rev. **46**, 3962–3979 (2017)

Link, S., El-Sayed, M.A.: Optical properties and ultrafast dynamics of metallic nanocrystals. Annu. Rev. Phys. Chem. **54**, 331–366 (2003)

Liu, J., Jalali, M., Mahshid, S., Wachsmann-Hogiu, S.: Are plasmonic optical biosensors ready for use in point-of-need applications? Analyst **145**, 364–384 (2020)

Lu, X., Ye, G., Deep, P., Chiechi, R.C., Orrit, M.: Quantum yield limits for the detection of single-molecule fluorescence enhancement by a gold nanorod. ACS Photon. **7**, 2498–2505 (2020)

Luan, J., Morrissey, J.J., Wang, Z., Derami, H.G., Liu, K.K., Cao, S., Jiang, Q., Wang, C., Kharasch, E.D., Naik, R.R., Singamaneni, S.: Light: science & applications **7**, 29 (2018)

Maier, S.A.: Plasmonics: Fundamentals and Applications. Publisher, Springer, USA (2007)

Matveeva, E.G., Gryczynski, Z., Malicka, J., Lukomska, J., Makowiec, S., Berndt, K.W., Lakowicz, J.R., Gryczynskia, I.: Directional surface plasmon-coupled emission: application for an immunoassay in whole blood. Anal. Biochem. **344**, 161–167 (2005)

Mishra, P., Debnath, A.K., Dutta Choudhury, S.: Titanium nitride as an alternative and reusable plasmonic substrate for fluorescence coupling. Phys. Chem. Chem. Phys. **24**, 6256–6265 (2022)

Naik, G.V., Shalaev, V.M., Boltasseva, A.: Alternative plasmonic materials: beyond gold and silver. Adv. Mater. **25**, 3264–3329 (2013)

Neumann, T., Johansson, M.-L., Kambhampati, D., Knoll, W.: Surface-plasmon fluorescence spectroscopy. Adv. Funct. Mater. **12**, 575–586 (2002)

Okamoto, K., Funato, M., Kawakami, Y., Tamada, K.: High-efficiency light emission by means of exciton–surface-plasmon coupling. J. Photochem. Photobiol. C Photochem. Rev. **32**, 58–77 (2017)

Orozco, C.A., Liu, J.G., Knight, M.W., Wang, Y., Day, J., Nordlander, P., Halas, N.J.: Fluorescence enhancement of molecules inside a gold nanomatryoshka. Nano Lett. **14**, 2926–2933 (2014)

Pang, Y., Rong, Z., Wang, J., Xiao, R., Wang, S.: A fluorescent aptasensor for H5N1 influenza virus detection based-on the core–shell nanoparticles metal-enhanced fluorescence (MEF). Biosens. Bioelect. **66**, 527–532 (2015)

Ray, K., Badugu, R., Lakowicz, J.R.: Distance-dependent metal-enhanced fluorescence from Langmuir Blodgett monolayers of alkyl-NBD derivatives in silver island films. Langmuir **22**, 8374–8378 (2006)

Rycenga, M., Cobley, C.M., Zeng, Z., Li, W., Moran, C.H., Zhang, Q., Qin, D., Xia, Y.: Controlling the synthesis and assembly of silver nanostructures for plasmonic applications. Chem. Rev. **111**, 3669–3712 (2011)

Sathish, S., Kostov, Y., Rao, G.: High-resolution surface plasmon coupled resonant filter for monitoring of fluorescence emission from molecular multiplexes. Appl. Phys. Lett. **94**, 223113 (2009)

Schuller, J.A., Barnard, E.S., Cai, W., Jun, Y.C., White, J.S., Brongersma, M.L.: Plasmonics for extreme light concentration and manipulation. Nat. Mat. **9**, 193–204 (2010)

Semeniak, D., Cruz, D.F., Chilkoti, A., Mikkelsen, M.H.: Plasmonic fluorescence enhancement in diagnostics for clinical tests at point-of-care: a review of recent technologies. Adv. Mater. 2107986 (2022)

Song, H.Y., Wong, T.I., Guo, S., Deng, J., Tan, C., Gorelik, S., Zhou, X.: Nanoimprinted thrombin aptasensor with picomolar sensitivity based on plasmon excited quantum dots. Sens Actuat. B Chem. **221**, 207–216 (2015)

Su, Q., Wesner, D., Schönherr, H., Nöll, G.: Molecular beacon modified sensor chips for oligonucleotide detection with optical readout. Langmuir **30**, 14360–14367 (2014)

Su, Q., Jiang, C., Gou, G., Long, Y.: Surface plasmon-assisted fluorescence enhancing and quenching: from theory to application. ACS Appl. Bio Mater. **4**, 4684–4705 (2021)

Wang, Y., Huang, C.J., Jonas, U., Wei, T., Dostalek, J., Knoll, W.: Biosensor based on hydrogel optical waveguide spectroscopy. Biosens. Bioelectron. **25**, 1663–1668 (2010)

Wang, R., Zhang, D., Zhu, L., Wen, X., Chen, J., Kuang, C., Liu, X., Wang, P., Ming, H., Badugu, R., Lakowicz, J.R.L.: Selectable surface and bulk fluorescence imaging with plasmon-coupled waveguides. J. Phys. Chem. C **119**, 22131–22136 (2015)

Wang, M., Wang, M., Zheng, G., Dai, Z., Ma, Y.: Recent progress in sensing application of metal nanoarchitecture-enhanced fluorescence. Nanoscale Adv **3**, 2448–2465 (2021)

Winkler, P.M., Regmi, R., Flauraud, V., Brugger, J., Rigneault, H., Wenger, J., García-Parajo, M.F.: Optical antenna-based fluorescence correlation spectroscopy to probe the nanoscale dynamics of biological membranes. J. Phys. Chem. Lett. **9**, 110–119 (2018)

Xu, L.T., Chen, M., Weng, Y.H., Xie, K.X., Wang, J., Cao, S.H., Li, Y.Q.: Label-free fluorescent nanofilm sensor based on surface plasmon coupled emission: in situ monitoring the growth of metal−organic frameworks. Anal. Chem. **94**, 6430–6435 (2022)

You, C.Y., Lin, L.H., Wang, J.Y., Zhang, F.L., Radjenovic, P., Yang, Z., Tian, Z.Q., Li, J.F.: Plasmon-enhanced fluorescence of phosphors using shell-isolated nanoparticles for display technologies. ACS Appl. Nano Mater. **3**, 5846–5854 (2020)

Yu, H., Peng, Y., Yang, Y., Li, Z.Y.: Plasmon-enhanced light-matter interactions and applications. Npj Comput Mater **5**, 45 (2019)

Zang, F., Su, Z., Zhou, L., Konduru, K., Kaplan, G., Chou, S.Y.: Ultrasensitive Ebola virus antigen sensing via 3D nanoantenna arrays. Adv. Mater. 1902331 (2019)

Zhang, J., Fu, Y., Mahdavi, F.: Bimetallic nanoshells for metal-enhanced fluorescence with broad band fluorophores. J. Phys. Chem. C **116**, 24224–24232 (2012)